Replication Protein A Interactions with DNA: Differential Binding of the Core Domains and Analysis of the DNA Interaction Surface†

Iwona M. Wyka,‡ Kajari Dhar,‡ Sara K. Binz, and Marc S. Wold*

Department of Biochemistry, University of Iowa College of Medicine, 51 Newton Road, Iowa City, Iowa 52242-1109

Received May 30, 2003; Revised Manuscript Received September 9, 2003

ABSTRACT: Human replication protein A (RPA) is a heterotrimeric (70, 32, and 14 kDa subunits), eukaryotic single-stranded DNA (ssDNA) binding protein required for DNA recombination, repair, and replication. The three subunits of human RPA are composed of six conserved DNA binding domains (DBDs). Deletion and mutational studies have identified a high-affinity DNA binding core in the central region of the 70 kDa subunit, composed of DBDs A and B. To define the roles of each DBD in DNA binding, monomeric and tandem DBD A and B domain chimeras were created and characterized. Individually, DBDs A and B have a very low intrinsic affinity for ssDNA. In contrast, tandem DBDs (AA, AB, BA, and BB) bind ssDNA with moderate to high affinity. The AA chimera had a much higher affinity for ssDNA than did the other tandem DBDs, demonstrating that DBD A has a higher intrinsic affinity for ssDNA than DBD B. The RPA−DNA interface is similar in both DBD A and DBD B. Mutational analysis was carried out to probe the relative contributions of the two domains to DNA binding. Mutation of polar residues in either core DBD resulted in a significant decrease in the affinity of the RPA complex for ssDNA. RPA complexes with pairs of mutated polar residues had lower affinities than those with single mutations. The decrease in affinity observed when polar mutations were combined suggests that multiple polar interactions contribute to the affinity of the RPA core for DNA. These results indicate that RPA−ssDNA interactions are the result of binding of multiple nonequivalent domains. Our data are consistent with a sequential binding model for RPA, in which DBD A is responsible for positioning and initial binding of the RPA complex while DBD A together with DBD B direct stable, high-affinity binding to ssDNA.

Human replication protein A (RPA)[1] is a single-stranded DNA binding protein composed of 70, 32, and 14 kDa subunits (RPA70, RPA32, and RPA14, respectively; for recent general reviews, see refs *1* and *2*). RPA was first identified as a human cell factor that is essential for cell-free SV40 replication (*3*−*5*). RPA homologues have been identified in all eukaryotes that have been examined (*1*, *2*, *6*). All RPA homologues bind to ssDNA with high affinity and participate in specific protein−protein interactions (*1*, *2*, *6*). The three subunits of RPA are required for proper function: all three genes encoding subunits of the RPA homologue are essential for viability of *Saccharomyces cerevisiae* (*7*, *8*). The heterotrimeric RPA complex is required for cellular DNA replication, repair, and recombination. RPA is needed for the cellular response to DNA damage and associates with several proteins that regulate gene expression (*1*, *2*).

The three subunits of RPA are composed of six copies of a structurally conserved DNA binding motif termed an oligonucleotide/oligosaccharide binding fold or OB-fold. This fold is found in proteins that bind ssDNA or oligosaccharides. OB-folds consist of five β-strands, which form a closed β-barrel with an α-helix between the third and fourth strands (*9*). The OB-folds found in RPA have been identified by a combination of sequence analysis and structural studies (*10*−*14*). OB-folds are also found in single-stranded DNA binding proteins of bacteria and bacteriophages, suggesting that the mechanism of ssDNA binding is evolutionarily conserved. The six domains consisting of an OB-fold are designated DNA binding domains (DBDs) A−F. These DBD domains are involved in both RPA−protein and RPA−DNA interactions.

RPA70 is composed of four OB-fold domains [DBD F and A−C (Figure 1)]. The N-terminal domain of RPA70, DBD F, has been shown to interact with multiple proteins and to bind DNA weakly (*15*, *16*). DBD F is connected to DBD A by an extended, ∼60-amino acid flexible linker (*16*). DBD A and B comprise the high-affinity, single-stranded DNA binding core (*17*). The C-terminus of RPA70, DBD C, has been shown to contribute minimally to ssDNA binding and to interact specifically with damaged DNA (*18*). DBD C contains a highly conserved zinc finger motif, which seems to be important for DNA damage recognition and interactions with the 3′-end of nascent DNA (*18*, *19*).

† These studies were supported by Grant GM44721 from the General Medicine Institute of the National Institutes of Heath.

* To whom correspondence should be addressed. Phone: (319) 335-6784. Fax: (319) 384-4770. E-mail: marc-wold@uiowa.edu.

‡ These authors contributed equally to this work.

[1] Abbreviations: RPA, human replication protein A; RPA70, 70 kDa subunit of RPA; RPA32, 32 kDa subunit of RPA; RPA14, 14 kDa subunit of RPA; DBD, DNA binding domain; dsDNA, double-stranded DNA; $(dT)_{30}$, oligodeoxythymidine 30 residues in length; $(dT)_{70}$, oligodeoxythymidine 70 residues in length; GMSA, gel mobility shift assay; His, histidine tag; nt, nucleotide; OB-fold, oligosaccharide/oligonucleotide binding fold; SSB, single-stranded DNA binding protein; ssDNA, single-stranded DNA.

10.1021/bi034930h CCC: $25.00
Published on Web 10/15/2003

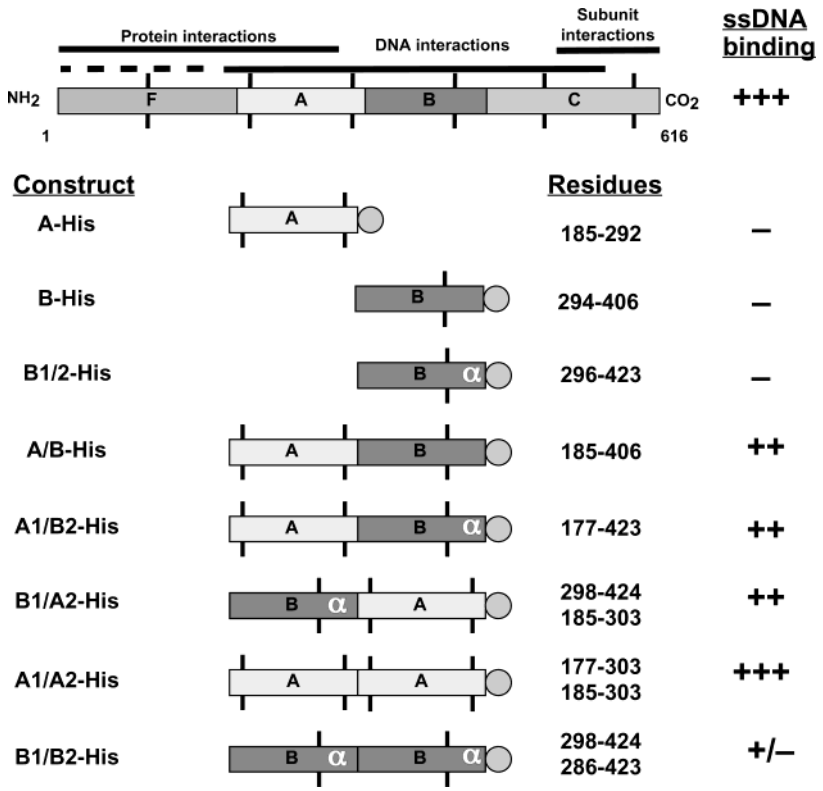

FIGURE 1: Schematic of DBD constructs. This figure depicts a graphical representation of RPA70 and the DBD constructs made for this study. A schematic of RPA70 (top) shows domains and known functions. Schematics of each DBD construct that was created are shown below. The abbreviated name of each construct and amino acids that are included are indicated. The right column indicates ssDNA binding activity of each DBD construct; the number of + signs indicates relative activity, and a − sign indicates no binding detected. A circle indicates the location of the six-histidine tag; α indicates the presence of the C-terminal α-helix located in DBD B.

RPA function requires specific interactions with a number of cellular proteins. RPA interacts with proteins involved in DNA replication (large tumor antigen and DNA polymerase α-primase complex), repair (XPA/XPG and UDG), recombination (RAD52), and transcription (GAL4 and VP16) (*1*, *2*). These interactions are essential for DNA repair, recombination, and the initiation and elongation phases of DNA replication (*1*, *2*). DBD A and F in RPA70 interact with both proteins and DNA, suggesting that there is competition between some DNA and protein interactions.

The primary RPA−DNA interaction is with ssDNA; however, RPA function requires interactions with other forms of DNA. RPA binds to damaged DNA and double-stranded (ds) DNA and can destabilize dsDNA helices. We have shown that both dsDNA binding and helix destabilization activities are manifestations of ssDNA binding activity (*20*). RPA binds to ssDNA with high affinity ($K_a \sim 10^{10}$ M^{-1}) (*21*, *22*). RPA exhibits low specificity for specific sequences with a 50-fold preference for polypyrimidine tracks (*21*). This sequence preference is similar to those of other nonspecific ssDNA binding proteins (*32*). RPA−ssDNA binding is length-dependent; binding affinity varies 200-fold from $\sim 7 \times 10^7$ M^{-1} for $(dT)_{10}$ to $\sim 1.5 \times 10^{10}$ M^{-1} for $(dT)_{50}$ (*21*). Compared to prokaryotic and viral ssDNA binding proteins (SSB), such as *Escherichia coli* SSB, RPA exhibits low cooperativity in DNA binding (*22*).

Deletion analysis and molecular analysis have identified a high-affinity ssDNA binding site in the center of RPA70 (*1*, *2*). This high-affinity DNA binding core consists approximately of residues 170−445 (DBD A and B, Figure 1) and is necessary and sufficient for high-affinity ssDNA binding (*17*). The other DNA binding domains in RPA also contribute to the affinity of the RPA complex for DNA (*17*). The crystal structure of the core DNA binding domain has been determined in a complex with $(dC)_8$ (*11*). The interaction surface of the RPA core binding site consists of a combination of 18 polar and nonpolar residues (*11*). In this surface, there are polar interactions with the phosphate backbone and the bases and nonpolar, base stacking interactions between aromatic residues and the bases (*11*). In addition, the interaction surface seems to be dynamic and involves multiple nonspecific interactions with DNA (*23*). Studies in *S. cerevisiae* also identified DBD A and B in yeast RPA70 as being essential for cell viability (*10*) and DNA binding (*24*). These studies also indicated that DBD A and B were not functionally equivalent; yeast cells were found to be viable when the RPA70 gene contained two tandem copies of DBD A, but not when two tandem copies of DBD B were inserted in place of DBD A and B (*10*). These data argue that DBD A of yeast RPA has at least one essential function that is not present in DBD B (*10*).

The molecular mechanism by which RPA binds to ssDNA is still not understood. Although interacting residues in the RPA core have been mapped by X-ray crystallography and NMR (*11*, *23*), the contribution of individual interactions has not been defined. Furthermore, the DBDs of RPA are structurally conserved, yet they are not genetically equivalent. Understanding the RPA−ssDNA interaction requires detailed characterization of the high-affinity binding core of RPA70. In these studies, we define the DNA binding properties of DBD A and DBD B. We show that DBD A and B have different affinities for ssDNA, with DBD A having a

Table 1: DBD Construct Characteristics

full name of DBD construct	abbreviated name	residues	predicted mass (kDa)	determined mass (kDa)[a]	sedimentation coefficient[b]
RPA70(185−292)-His	A-His	185−292	13.6	13.5	1.4 ± 0.2
RPA70(294−406)-His	B-His	294−406	13.7	13.7	1.5 ± 0.2
RPA70(298−422)-His	B1/2-His	298−422	15.1	15.1	1.5 ± 0.1
RPA70(185−406)-His	A/B-His	185−406	26.1	26.1	2.5 ± 0.2
RPA70(179−422)-His	A1/B2-His	179−422	28.6	28.5	2.6 ± 0.1
RPA70(298−424:185−303)-His	B1/A2-His	298−424 and 185−303	29.5	29.5	2.5 ± 0.2
RPA70(179−298:181−303)-His	A1/A2-His	179−424 and 181−303	29.2	29.1	2.7 ± 0.1
RPA70(298−424:301−422)-His	B1/B2-His	298−424 and 301−422	28.7	28.7	2.5 ± 0.1

[a] Determined by MALDI-TOF mass spectroscopy analysis at the Molecular Analysis Facility at The University of Iowa. [b] Sedimentation coefficients of the RPA70 core DBD constructs were determined by glycerol gradient sedimentation as described previously (*21*).

significantly higher affinity than DBD B. We also show by mutational analysis that polar interactions contribute more to the apparent affinity of the human RPA complex than do nonpolar base stacking interactions. Finally, all polar residue mutations generated in these studies caused a significant decrease in the affinity of the RPA complex for DNA. Furthermore, RPA complexes with pairwise combinations of point mutations had lower affinities than the single-residue mutants, suggesting that the high affinity of RPA is the result of a combination of multiple weak interactions.

MATERIALS AND METHODS

Materials. Plasmid MiniPrep, PCR purification, and gel purification kits used in DNA manipulations were purchased from Qiagen. The Taq polymerase used in PCRs was purchased from Invitrogen. Other PCR components were obtained from the DNA Core Facility at The University of Iowa (Iowa City, IA). The DNA ligase was purchased from New England BioLabs. The [γ-^{32}P]ATP (4500 Ci/mmol) was purchased from Amersham. The $(dT)_{30}$ and $(dT)_{70}$ oligonucleotides were obtained from Bio-Synthesis, Inc. The T4 polynucleotide kinase (T4-PNK) was purchased from Life Technologies, Inc. The Micro Bio-Spin columns used for labeled oligonucleotide purification were bought from Bio-Rad. The Ni−NTA Superflow resin and imidazole were purchased from Qiagen and Sigma, respectively.

HI buffer contains 30 mM HEPES (diluted from a 1 M stock at pH 7.8), 1 mM dithiothreitol (DTT), 0.25 mM EDTA, 0.5% (w/v) inositol, and 0.01% (v/v) Nonidet P-40 (termed HI-0). HI buffer was supplemented with indicated concentrations of KCl or imidizole.

The 1× FBB (filter binding buffer) used in GMSA reactions contained 30 mM HEPES (diluted from a 1 M stock at pH 7.8), 100 mM NaCl, 5 mM $MgCl_2$, 0.5% inositol, and 1 mM DTT. The Tris-acetate/EDTA gel buffer (TAE being 40 mM Tris-acetate and 2 mM EDTA at pH 8.5) was used at a concentration of 1× for DNA gels and a concentration of 0.1× for GMSA gels (*25*). The buffer used for protein gels contained 0.1% (SDS), 25 mM Tris base, and 192 mM glycine.

DBD Constructs. All RPA70 DNA binding domain (DBDs) constructs were generated using PCR to amplify specific regions of the RPA70 cDNA. The following is a list of primers (and constructs made with each): #162-B-5′*Nco*I, 5′-ATGCCCTGGAATTCCATGGATCTTTACCTACGGTT-3′ (B-His and A/B-His); #286-A-3′*Xho*I, 5′-CTGAGGTAACTCGAGGTCGTCCTCACAGGGC-3′ (A-His and A/B-His); #287-A-5′*Nco*I, 5′-ACACAGTCCACCATGGTGCCCATTGCCAGCC-3′ (A-His and A/B-His); #288-B-3′*Eag*I, 5′-GCTTATACGGCCGGGTGTCAGGATTCGC-3′ (B-His and A/B-His); #290-(A1)-3′*Bam*HI, 5′-CGTGAAATCGGATCCAACCGTAGGTAA-3′ (A1/B1-His and A1/A2-His); #291-(A2)-5′*Bam*HI, 5′-CACACATCTGCGGGATCCCAGTCCAAAGTG-3′ (B1/A2-His and A1/A2-His); #292-(A1)-5′*Nco*I, 5′-CACACTTCCATGGGAACACAGTCC-3′ (A1/B1-His and A1/A2-His); #295-(B2)-3′*Eag*I, 5′-GATGGAAACGGCCGCTAAGGCTTGTCCTTC-3′ (B1/B2-His and A1/B2-His); #296-(B2)-5′*Bam*HI, 5′-CTACCAACAGTTGGATCCGATTTCACGGGGAT-3′ (B1/B2-His and A1/B2-His); #297-(B1)-5′*Nco*I, 5′-CATCATTTACCCATGGTTCAGTTTGATTTCACG-3′ (B1/B2-His and B1/A2-His); #298-(B1)-3′*Bam*HI, 5′-TAGATTAGGGATGGATCCACCATCTAAGGC-3′ (B1/B2-His and B1/A2-His); and #299-(A2)-3′*Eag*I, 5′-GTCATCAACGGCCGTGAAATCAAACTG-3′ (B1/A2-His and A1/A2-His).

Desired domains of the RPA70 gene were first amplified by PCR, and the resulting DNA fragment was cut with appropriate restriction enzymes and ligated with the precut, purified pET28a vector. This introduced a six-histidine tag in frame at the C-terminus of each coding sequence. Constructs were generated using pl1d-RPA70 (*26*) as a PCR template and amplified with Taq polymerase using primers as indicated above. Each construct that was generated contained an *Nco*I (5′) site (nucleotide base changes underlined to generate a *Nco*I restriction site used as the ATG initiation codon), *Eag*I (3′) site, and internal *Bam*HI site (in the case of tandem constructs). The desired sets of PCR products were digested with the indicated restriction enzymes and ligated into the pET28a vector predigested with *Nco*I and *Eag*I. Each generated plasmid contained a T7 promoter, a Shine-Dalgarno ribosome binding site, and the coding sequence of a RPA70 core DBD construct followed by a C-terminal histidine tag (His tag). Expression vectors for A-His and B-His were made following a similar procedure (*27*). RPA70 DBD constructs that were made are summarized in Table 1. Each DBD construct was named for the RPA subunit and the amino acids included; for example, RPA70-(185−292)-His contains amino acids 185−292 of RPA70. The sequence of all constructs was confirmed by DNA sequencing.

Construction of RPA70 Point Mutants. p11d-tRPA, which directs the expression of all three subunits of RPA (*26*), was used as the template for mutagenesis. Selected amino acids that interact with DNA in DBD A and B were mutated to alanine by Quick Change site-directed mutagenesis (Stratagene) using the following primer pairs (nucleotide changes

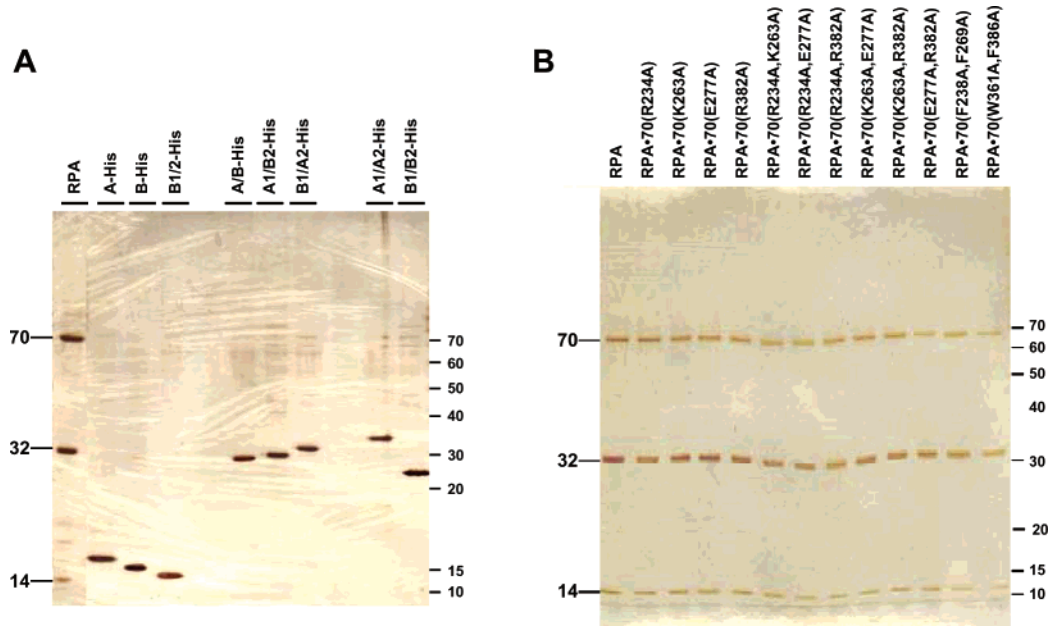

FIGURE 2: Purified forms of RPA used in these studies. A 0.5−1 μg sample of purified RPA, DBD constructs (A) or mutant forms of the RPA complex (B), was separated by electrophoresis on an 8 to 14% SDS−PAGE gel and visualized by staining with silver nitrate. Positions of the wild-type RPA subunits and molecular markers are shown on the left and right side of each panel, respectively. Molecular masses are given in kilodaltons.

underlined): RPA70(R234A), 5′-GGTGAAATCGCGGC-TACAGCTTTTAAAGAGCAA-3′ and 5′-TTGCTCTTTA-AAAGCTgTAGCCGCGATTTCACC-3′ (creating a *Dra*I site); RPA70(K263A), 5′-TATTTCTCGAAAGGGACCCTG-GCGATTGCTAACAAG-3′ and 5′-CTTGTTAGCAATCGC-CAGGGTCCCTTTCGACAAATA-3′ (creating an *Ava*II site); RPA70(E277A), 5′-GTTAAAAATGACTACGCGAT-GACCTTTAAAAACGAG-3′ and 5′-CTCGTTTTTAAAGT-TCATCGCGTAGTCATTTTTAAC-3′ (creating a *Dra*I site); and RPA70(R382A), 5′-GCTATCAAAGGCGCCGCCGT-CTCTGATTTC-3′ and 5′-GAAATCAGAGACGGGGCGTC-CTTTGATAGC-3′ (creating a *Kas*I site).

Double mutations were made by subjecting one of the four point mutants described above to a second round of mutagenesis using a second set of primers (listed above). Double aromatic point mutants [RPA70(F238A/F269A) and RPA70-(W361A/F386A)] were made by subjecting plasmids directing the expression of single-aromatic residue mutations, ptRPA70(F238A) and ptRPA70(W361A) (*17*), to a second round of mutagenesis as described above using the mutagenic primers for residues F269 and F386 described previously (*17*). All mutations were confirmed by DNA sequencing.

Protein Expression and Purification. Individual RPA70 domain constructs were expressed in BL21(DE3) cells and lysed as described previously (*17*). The histidine-tagged proteins were then purified at 4 °C using a 10 mL column of Ni−NTA Superflow resin. The recombinant protein was eluted using a 100 mL gradient from HI-100 KCl with 10 mM imidazole to HI-100 KCl with 500 mM imidazole. All of the RPA70 domain constructs eluted at an imidazole concentration of ∼100 mM. The protein concentration was calculated using a Bradford assay with bovine serum albumin as a standard. Protein purity was assessed by analysis on an SDS−polyacrylamide gel followed by staining with silver nitrate. Wild-type and mutant forms of the RPA complex were purified as described previously (*17*).

Gel Mobility Shift Assay (GMSA). Oligonucleotides, $(dT)_{30}$ or $(dT)_{70}$, were labeled with [γ-^{32}P]ATP by T4 polynucleotide kinase (*28*). The labeled DNA was separated from free ATP with a P-30 Micro Bio-Spin Tris chromatography column by following the manufacturer's protocol. GMSAs were performed as described previously (*28*). Each 15 μL reaction mixture contained 1× FBB, 0.1 fmol of DNA, and the indicated amount of the wild-type or mutant form of RPA. Binding reaction mixtures were incubated for 20 min at 25 °C. The mixtures were then brought to final concentrations of 4% glycerol and 0.01% bromophenol blue and separated on a 1% agarose gel in 0.1× TAE buffer. The gels were then dried on DE81 paper, and radioactive bands were visualized by autoradiography. The radioactivity in each band was quantitated using the Packard Instant Imager. The binding isotherms, used to calculate binding constants, were generated by plotting the fraction of free ssDNA versus RPA concentration in each reaction. The intrinsic binding constants were calculated by nonlinear least-squares fitting of the data to the Langmuir binding equation using KaleidaGraph (Synergy Software) as described previously (*21*).

RESULTS

Initial Characterization of RPA70 DBD Constructs. Previous analysis of human RPA70 identified four structurally similar but functionally divergent DNA binding domains [DBD F and A−C (Figure 1)]. We created a series of monomeric and tandem DBD constructs of the high-affinity binding core of RPA (Figure 1) to examine the contributions of individual DBDs to the total DNA binding affinity of RPA. All proteins were found to be expressed at high levels in *E. coli* and were predominantly present in the soluble fraction after cell lysis (data not shown). Nickel affinity chromatography yielded proteins that were highly purified (Figure 2A). The mass of each polypeptide was within 1% of its predicted mass, supporting the conclusion that the expressed proteins are the desired DBD constructs (Table

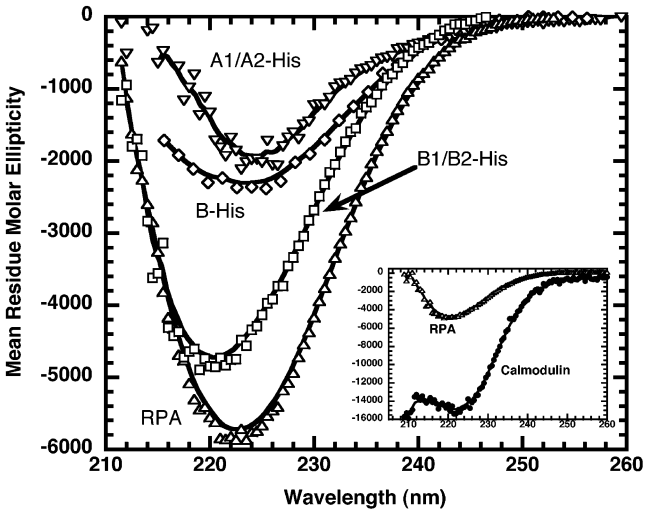

FIGURE 3: Circular dichroism scans. Graph summary of the CD scans obtained for the DBD constructs. Circular dichroism spectra were recorded from 260 to ~210 nm using an Olis CD module Cary-17 conversion spectrophotometer (Online Instrument Systems, Inc.) with a 1 cm path length quartz cuvette. Each protein sample was dialyzed for several days in CD buffer [20 mM $NaHPO_4$, 100 mM KCl, 20% sucrose (w/v), 10% glycerol (v/v), and 0.5 mM EDTA (pH7.5)] and concentrated using a Centricon concentrator (when necessary) prior to CD analysis. All spectra are the average of two scans and were repeated multiple times. Scans were obtained at 25 °C with a 3 mL sample of protein in a 1 cm cuvette. The mean residue molar ellipticity was plotted against wavelength (nanometers) for wild-type RPA (△), A1/A2-His (▽), B1/B2-His (□), B-His (◇), and rat calmodulin (●). The inset shows spectra of RPA and calmoulin with an expanded scale.

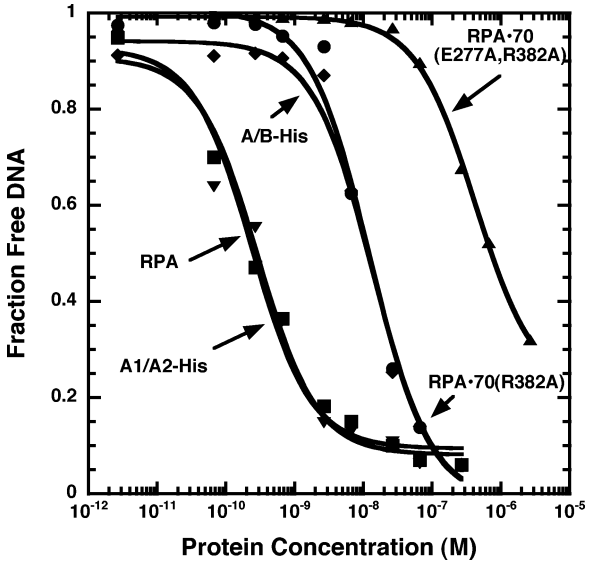

FIGURE 4: Representative binding isotherms for RPA, selected DBD constructs, and mutant RPA complexes. Binding to $(dT)_{30}$ was assessed by GMSAs. Binding data and best-fit curves for RPA (▼), A1/A2-His (■), A1/B2-His (◆), RPA70(R382A) (●) and RPA70-(E277A/R382A) (▲).

1). Each DBD construct was found to migrate as a single peak by velocity centrifugation and to have a sedimentation constant consistent with being a monomer in solution (Table 1). As expected, the sedimentation constant for the DBD constructs were significantly lower than the sedimentation constant (5.3 S) of the native trimeric RPA complex (*29*).

Whenever a mutation or a deletion is made in a protein, there is a concern that the change may perturb the overall protein structure. To address this concern, circular dichroism spectroscopy (CD) was used to analyze the secondary structure of each DBD construct. The OB-folds present in the DBDs of RPA are mostly composed of β-sheets with a small number of connecting α-helices. Therefore, the CD spectrum of RPA and the DBD constructs should be predominantly that of β-sheets. The CD spectrum of heterotrimeric RPA has a negative deflection with a single minimum between 220 and 230 nm (Figure 3). This is in contrast to the spectrum of the predominantly α-helical rat calmodulin which has a negative deflection with two minima (Figure 3, inset). The scans obtained for the DBD constructs also had a negative deflection between 220 and 230 nm consistent with a structure composed of a combination of α-helices and β-sheets, but not random coil (Figure 3 and data not shown). These spectra are not consistent with random coil or unfolded protein; we conclude that all constructs are folded. These data do not rule out the possibility that the constructs have a modified fold but suggest that their secondary structure is similar to that of wild-type RPA.

ssDNA Binding Properties of DBD Constructs. Binding of the DBD constructs to ssDNA was examined by gel mobility shift assays (GMSAs). In this assay, a short radiolabeled oligonucleotide is incubated with increasing concentrations of protein. The resulting protein−DNA complexes are separated from unbound DNA by gel electrophoresis, and the amount of radioactivity in each species is quantitated. The binding isotherm that is obtained can be analyzed to determine the apparent equilibrium binding constant. No stable complexes were observed with the monomeric DBDs and labeled $(dT)_{30}$ oligonucleotide (data not shown). In cross-linking studies, DBD A−DNA complexes were observed, suggesting that the monomeric DBD A construct is capable of binding to ssDNA (data not shown). This indicated that the binding affinity of the monomeric constructs is too low to be detected under these conditions and/or that the protein−DNA complex is not stable. Consistent with these data, monomeric DBD constructs of yeast RPA were also shown to have a low affinity for ssDNA; protein−DNA complexes were only observed after cross-linking (*30*).

Several tandem DBD constructs were made containing the core DNA binding domains. These include two core domains consisting of DBD A and B with different end points (A/B-His and A1/B2-His) and a reverse core construct with DBD B positioned prior to DBD A (B1/A2-His). The core constructs (A/B-His and A1/B2-His) bound to $(dT)_{30}$ with affinities of 7.3×10^7 and 14.5×10^7 M^{-1}, respectively (Figure 4 and Table 2). This is $^1/_{25}$ of that of wild-type RPA and is similar to the affinity observed for other RPA70 core constructs (Table 2; see also ref *17*). Previously studied core constructs did not contain histidine tags (*17*). The finding that A/B-His and A1/B2-His had the same binding affinity as the core domain without a histidine tag [RPA70(169−441) described in ref *17*] indicates that the histidine tag does not affect interactions of the core with DNA. This finding was confirmed with other RPA domain constructs (data not shown). A/B-His and A1/B2-His differ only by the presence of the α-helix at the C-terminus of DBD B. This helix appears to have no effect on ssDNA binding of these tandem

Table 2: ssDNA Binding of DBD Constructs

RPA form	K_a[(dT)$_{30}$] ($\times 10^8$ M^{-1})[a]	relative binding[b]	RPA form	K_a[(dT)$_{30}$] ($\times 10^8$ M^{-1})[a]	relative binding[b]
wild-type	25 ± 4	1.00	RPA70(R234A)	0.66 ± 0.27	0.027
A-His	≤0.0001	NA	RPA70(K263A)	4.5 ± 0.80	0.18
B-His	≤0.0001	NA	RPA70(E277A)	2.5 ± 0.60	0.10
B1/2-His	≤0.0001	NA	RPA70(R382A)	0.99 ± 0.17	0.040
A/B-His	0.73 ± 0.19	0.03	RPA70(R234A/K263A)	0.21 ± 0.10	0.009
A1/B2-His	1.4 ± 1.4	0.06	RPA70(R234A/E277A)	0.90 ± 0.004	0.036
B1/A2-His	1.4 ± 1.1	0.06	RPA70(R234A/R382A)	0.30 ± 0.02	0.012
A1/A2-His	59.0 ± 2.70	2.4	RPA70(K263A/E277A)	0.21 ± 0.04	0.009
B1/B2-His	≤0.001	NA	RPA70(K263A/R382A)	0.15 ± 0.095	0.006
RPA70(169−441)[c]	0.8 ± 0.2[c]	0.03[c]	RPA70(E277A/R382A)	0.09 ± 0.01	0.004
			RPA70(F238A/F269A)	5.7 ± 0.61	0.23
			RPA70(W361A/F386A)	3.6 ± 0.56	0.15

[a] Apparent association constants determined from GMSAs. Each value is the average of two or more independent titrations. The standard deviation (if average of three or more titrations) or variation (two titrations) is indicated for each value. [b] Relative binding ratio of K_a(mutant)/K_a(wild type). [c] RPA core binding domain constructed and binding analysis described by Walther *et al.* (*17*).

constructs. The reverse core construct (B1/A2-His) bound to DNA with the same affinity as the core constructs (Table 2), demonstrating that the position of DBD B has minimal effect on a construct's binding affinity.

The homo-tandem DBD constructs exhibited very different DNA binding properties. The binding affinity of the B1/B2-His construct was much lower than those of the core constructs. It was difficult to saturate the binding reaction mixtures even with high concentrations of B1/B2-His. Table 2 shows an upper limit of the estimated binding constant of B1/B2-His. In contrast, the A1/A2-His construct was able to bind (dT)$_{30}$ with an affinity of 6×10^9 M^{-1}, an affinity similar to that of wild-type RPA (Figure 4). Since the DNA concentration used in GMSA (~0.1 nM) is approximately equal to the apparent association constant of both wild-type RPA and A1/A2-His, binding was probably occurring under stoichiometric conditions. This means that the apparent association constants for both wild-type RPA and the double DBD A construct are not equilibrium binding constants and rather must be considered lower-limit estimates of the true equilibrium binding constants (Table 2). These data demonstrate that the affinity of A1/A2-His is much higher than that of B1/B2-His, and strongly suggest that these differences reflect the intrinsic binding properties of the two DBDs. These results indicate that the affinity of the core binding domain of RPA is a product of binding of two unequal DBDs. Although we have not directly examined the cooperativity of binding of the DBD constructs, the difference in apparent affinity between monomeric and tandem DBD constructs strongly suggests that the high affinity of the RPA core is a result of cooperative binding of the structurally linked domains.

The binding behavior of the monomeric and tandem DBD constructs was also examined with longer DNA. The monomeric DBD constructs did not bind (dT)$_{70}$ to a significant extent, even at high protein concentrations, indicating that the binding affinity must be less than 1×10^4 M^{-1} (data not shown). All of the tandem DBD constructs bound (dT)$_{70}$. As has been observed with wild-type RPA (*28*, *31*), two bands with altered mobility formed with the tandem DBD constructs at high protein concentrations (data not shown). This is consistent with multiple RPA molecules binding to the longer oligonucleotide. The binding constants obtained with (dT)$_{70}$ were similar to those found with (dT)$_{30}$: A1/A2-His binds strongest with an affinity close to that of wild-type RPA, the DBD A and B tandem constructs bind with reduced affinity (~$^1/_{50}$ of that of the wild type), and the B1/B2-His construct binds with a very low affinity (data not shown). These data are consistent with our conclusions that DBD A has a higher affinity for DNA than DBD B.

Mutational Analysis of the RPA−DNA Binding Surface. The finding that DBD A has a higher intrinsic affinity for DNA than DBD B suggests that these two domains could be contributing differently to the binding of the RPA complex. To explore the roles of the core binding domains in RPA binding to DNA, we carried out mutational analysis of polar and nonpolar residues in the RPA−DNA interface. Figure 5A shows the structure of the core DNA binding region with residues found to interact with DNA in the crystal structure highlighted (*11*). For our initial studies, we targeted four polar residues on the face of the DNA interaction surface: three in DBD A (R234, E277, and K263) and one in DBD B (R382) (Figure 5A). Individual point mutations were generated and expressed with the 32 and 14 kDa subunits to make mutant RPA complexes. All four mutant forms of RPA were purified to apparent homogeneity with high yield (Figure 2B).

To confirm that the mutations did not significantly disrupt the structure of the RPA complex, proteolytic analysis was performed. We have shown previously that partial proteolysis can be used to monitor the structure of the RPA complex (*31*) and that mutations that disrupt the structure of RPA perturb the proteolytic cleavage pattern (*17*). The digestion pattern obtained with the mutated RPA complexes was similar to that of wild-type RPA, suggesting that these mutations do not disrupt the global structure of the complex (data not shown). Gel mobility shift assays were used to analyze the binding of the mutant RPA complexes. Mutating any of the four polar residues decreased the DNA binding affinity of the RPA (Figure 4 and Table 2). The binding constant obtained for the three residues mutated in DBD A ranged from 4.5×10^8 to 6.6×10^7 M^{-1} (20 and 2% of that of the wild-type RPA complex). Interestingly, the mutation of a single polar residue in DBD B [RPA70(R382A)] had an affinity (9.9×10^7 M^{-1}) similar to that of the most severe mutation in DBD A [RPA70(R234A)] and to that of A1/B1-His (Figure 4). These studies confirm that point mutations in the DNA binding site of either DBD A or DBD B cause significant reductions in the affinity of the complex for DNA.

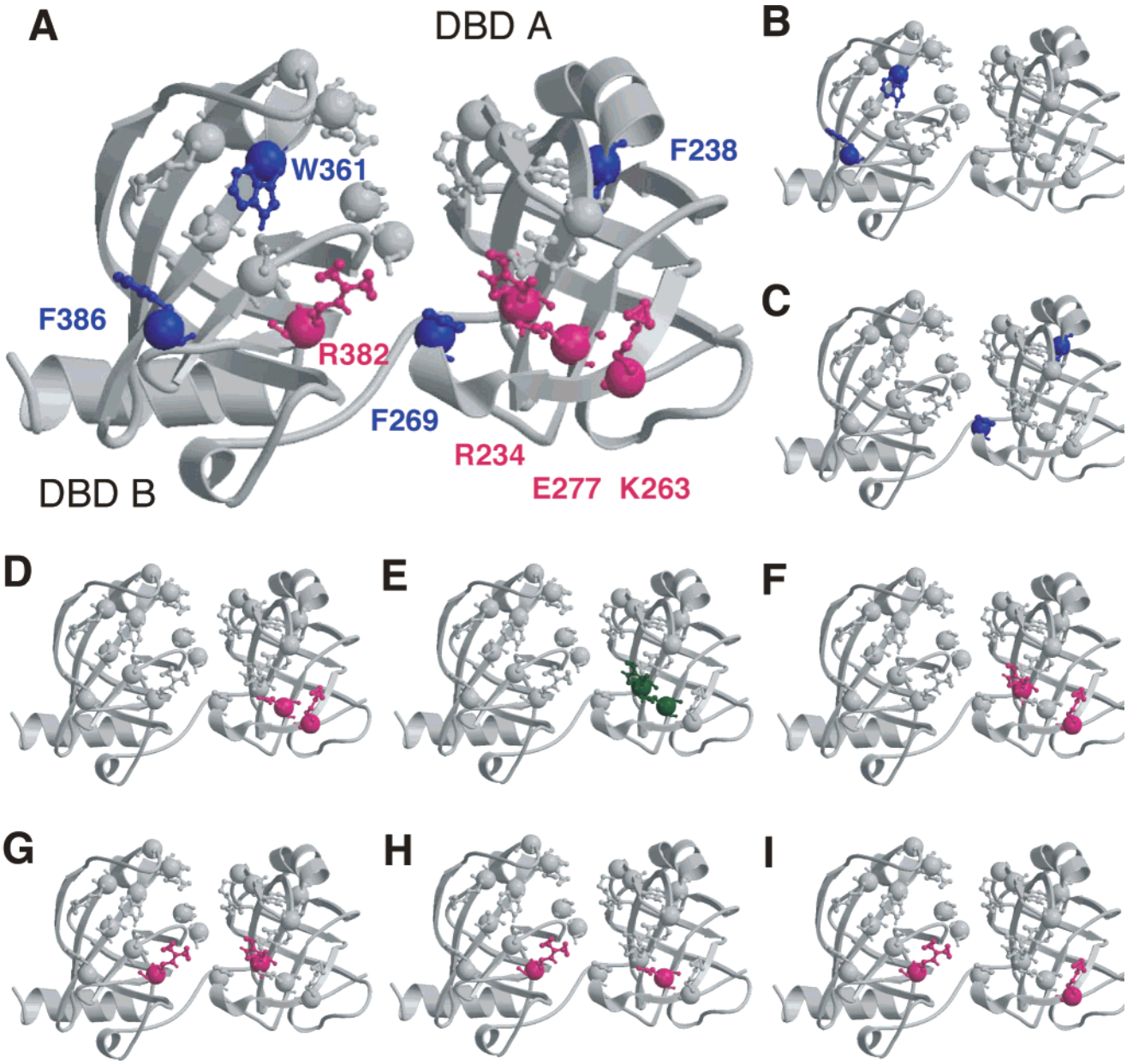

FIGURE 5: Core DNA binding domain with interacting residues and mutant pairs shown. Molecular models of the core DNA binding domain of RPA (DBD A and B) based on the crystal structure of the DNA-bound complex (*11*). (A) Core structure with residues found to interact with DNA indicated: mutated polar residues (pink), mutated aromatic residues (blue), and unmutated residues (light gray). DBD A, DBD B, and mutated residues are labeled. Other structures show double-mutant complexes studied: (B) RPA70(W361A/F386A), (C) RPA70(F238A/F269A), (D) RPA70(K263A/E277A), (E) RPA70(R234A/E277A), (F) RPA70(R234A/K263A), (G) RPA70(R234A/R382A), (H) RPA70(E277A/R382A), and (I) RPA70(K263A/R382A). Double-aromatic residue mutations are shown in blue, and double-polar residue mutations are shown in pink except for RPA70(R234A/E277A) which is shown in green to indicate the minimal effect of the double mutant.

The finding that point mutations in either DBD A or B dramatically lowered the affinity of the RPA complex confirmed that, even though the intrinsic affinity of the two DBDs differs, both contribute to the overall affinity of the RPA complex.

To further explore the binding of DBD A and B in the RPA complex, the four point mutations were combined to yield a series of six double mutants. The locations of the sites of mutation for each double mutant are shown in Figure 5D−I. These mutant forms of the RPA70 gene were coexpressed with the other two RPA subunits and the resulting RPA complexes purified (Figure 2B). Partial proteolysis did not indicate any major disruption of structure with any of the six double mutants (data not shown). Five of the double mutant complexes had apparent DNA binding constants that were less than 1% of that of the wild-type complex (Figure 6 and Table 2). These five mutant complexes had affinities for DNA that were significantly lower than those of any of the starting single-point mutations (Figure 6), suggesting that making two mutations in the interaction site has a cumulative effect on binding. The sixth double mutant, RPA70(R234A/E277A) (Figure 5E), had an affinity similar to that of RPA70(R234A). R234 and E277 are adjacent to each other on the interaction surface, and both interact with the same DNA base in the crystal structure (*11*). We postulate that the double mutant RPA70(R234A/E277A) displayed a smaller decrease in the level of binding because both mutations affect interactions with the same

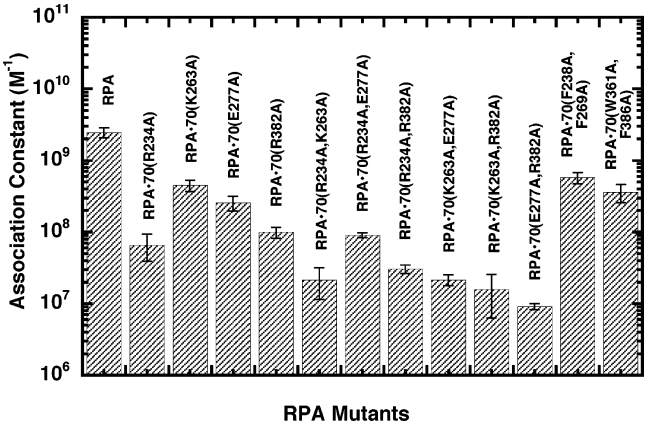

FIGURE 6: ssDNA binding activity of single- and double-point mutants in DBD A and B. Bar graph summarizing binding constants determined by GMSAs as described in Materials and Methods. Average apparent association constants determined from two or more binding experiments such as those shown in Figure 4; the experimental variation is indicated by error bars.

base. It is worth noting that K263 and E277 are also adjacent to each other in the DNA binding surface but interact with different sites on the DNA. When these two sites were mutated in RPA70(K263A/E277A) (Figure 5F), the effect on DNA binding was cumulative. These results suggest that the overall affinity of the RPA core for DNA is the result of a combination of the individual (probably weak) interactions. These studies also demonstrated that although DBD A and B have different intrinsic affinities for DNA, the binding affinity of the RPA complex depends on polar residues in both DBDs interacting with DNA.

There are four conserved aromatic residues in the RPA core, two in DBD A and two in DBD B [F238, F269, W361, and F386 (Figure 5A)]. These aromatic residues stack with bases in the RPA−DNA complex (*10*, *11*). Previous analysis of human RPA suggested that base stacking does not contribute significantly to the affinity of the RPA complex (*17*). In contrast, recent studies with yeast RPA (*24*) have suggested that mutation of both aromatic residues in a single DBD in yeast RPA disrupts the binding of that domain. Therefore, to determine whether mutation of both aromatic residues in a single DBD of human RPA would have properties similar to those of the homologous mutations in yeast RPA, two double mutants were made in which either both aromatic residues in DBD A or both aromatic residues in BDB B were mutated to alanine [RPA70(F238A/F269A) (Figure 5C) or RPA70(W361A/F386A) (Figure 5B), respectively]. These two mutant RPA complexes did not appear to have large disruptions in their structure, unlike the double aromatic mutant form of RPA [RPA70(F238A/W361A)] characterized previously (*17*). These double mutations decreased the affinity of the RPA complex by less than 1 order of magnitude (Table 2). This is consistent with our previous studies of human RPA which found that the single-aromatic residue mutations and RPA70(F269A/F386A) had minimal effects on ssDNA binding (*17*), These data indicate that mutation of the aromatic residues had a much smaller effect on the affinity of the human RPA complex for DNA than did mutation of the polar residues discussed above. We conclude that for the human RPA complex, the aromatic residues only make a minor contribution to the affinity of the RPA complex for DNA. This suggests that there are significant differences in the interactions between human and yeast RPA complexes and DNA.

DISCUSSION

This study investigated the roles of individual DBDs in the RPA core in ssDNA binding. The tandem construct A1/A2-His had an affinity close to that of wild-type RPA ($\sim 10^9$ M^{-1}); the core and reverse core constructs had an affinity of $\sim 10^8 - 10^7$ M^{-1}, while the binding affinity of B1/B2-His was estimated to be $\leq 10^6$ M^{-1}. We propose that the difference in binding affinity of the two double-domain constructs is the result of an intrinsic difference in the DNA binding activity of these two DNA binding domains. Interestingly, the level of evolutionary conservation of DBD A is much higher than the level of conservation of DBD B (S. K. Binz, unpublished data). This suggests that some property of DBD A, such as high-affinity DNA binding, is evolutionarily important for RPA's function.

The crystal structure of the high-affinity DNA binding domain bound to DNA suggests that both hydrophobic (base stacking) and ionic interactions contribute to the stability of the RPA−DNA complex (*11*). In the crystal structure, four aromatic residues and 14 polar residues are observed interacting with ssDNA. The polar residues interact directly with the bases and/or with the phosphate backbone. Interestingly, there are more interacting residues in DBD B (10) than there are in DBD A (8) (*11*). Recent NMR studies suggested that the DNA interaction surface of RPA is flexible and implicated additional residues as being involved in RPA−DNA interactions (*23*). Our mutational analyses demonstrate that even though there is a difference in the intrinsic affinity of DBD A and DBD B, individual polar residues in both DBDs contribute to the high-affinity binding of RPA to ssDNA. This conclusion is consistent with the strong ionic dependence of RPA binding to ssDNA (*22*) and also with studies of other single-stranded DNA-binding proteins that exhibit multiple ionic interactions (*32*). We also show that mutation of polar residues has a greater effect on the affinity of these chimeras than does mutation of aromatic residues. This suggests that polar interactions, not base stacking, are principally responsible for the high affinity of RPA for ssDNA.

From these studies, we conclude that individually each DBD has a low affinity for DNA and that the intrinsic affinities of individual DBDs differ. We propose that when DBDs are combined in pairs or higher multimers, cooperative binding results in a high-affinity complex. This indicates that multiple DBDs are essential for high-affinity ssDNA binding. Support for this model comes from the binding properties of the monomeric and tandem DBD constructs. It is also supported by the number and location of DBDs in RPA and the observation that other ssDNA binding proteins (e.g., tetrameric *E. coli* SSB and BRCA2) also contain multiple DBDs (*33*−*36*). An alternative model is one in which multiple DBDs are required for individual DBDs to fold optimally. The CD spectrum of the monomeric constructs (Figure 3 and data not shown) and the finding that monomeric DBD F has been found to be an OB-fold in solution argue against this.

Our analysis indicates that DBD A and DBD B interact differently with ssDNA. These interactions are likely to allow

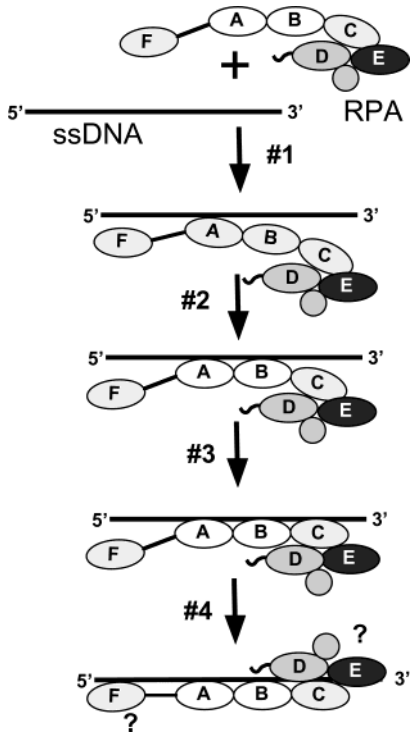

FIGURE 7: Hypothetical sequential model of RPA binding to ssDNA. DBDs are indicated by letters; the wavy line indicates the N-terminal phosphorylation domain of RPA32, and the circle indicates the C-terminal domain of RPA32. See Discussion for details.

RPA to play diverse roles in cellular DNA metabolism. Despite interspecies differences between DBD A and DBD B, the core of yeast RPA70 has been successfully replaced with the homologous regions of both human and rice RPA and found to support yeast viability (*10*, *37*). Thus, replacement of the RPA70 core DNA binding region with that from another RPA homologue appears to be less detrimental than individual domain swaps. Our finding that DBD A and B have different DNA binding properties provides an explanation for the interspecies domain exchange data.

The experiments presented here indicate that while DBD A and B are both essential for binding of the RPA 70 core, DBD A probably directs binding of the RPA complex. Additional support for this binding model comes from other studies. Analyses of the polarity of RPA binding to DNA showed that a strong interaction domain of RPA positioned at the 5′-side of the ssDNA binding region is required for the initial binding to ssDNA (*38*). The direction of the ssDNA in the crystal structure of the core DNA binding region is consistent with DBD A being the strong binding site and DBD B being the weaker binding site (*11*). Furthermore, Iftode and Borowiec (*39*) showed that there is polarity associated with RPA−ssDNA binding. They observed that binding initially occurs at the 5′-side of ssDNA and extends in the 3′-direction, consistent with DBD A being the first domain to bind to ssDNA.

Kinetic analysis of the binding of RPA to DNA has been minimal (*40*). However, several researchers have suggested that the RPA core directs RPA binding and that the DBDs bind sequentially (*38*). Our results are consistent with this hypothetical sequential binding model of RPA binding to ssDNA (Figure 7). The finding that DBD A has a higher affinity is consistent with DBD A of RPA70 initially interacting with ssDNA (#1 in Figure 7). The tight linkage between DBD A and B and the relatively high affinity of the DBD A−B core for ssDNA (*17*) suggest that together DBD A and B bind to give an initial, stable RPA−DNA complex (#2). We postulate that core binding then allows other DBDs in RPA to interact with the DNA. DBD C binds preferentially to certain types of damaged DNA and to the 3′-end of nascent DNA (*19*, *41*). Thus, DBD C would be expected to bind adjacent to the RPA core depending upon the length ssDNA (#3) (*19*, *41*). DBD C probably also directs binding to single-stranded, damaged DNA. DBD F and D have been shown to interact with DNA and may interact with specific forms of DNA during DNA metabolism (#4). For example, RPA32 (DBD D) has been shown to bind to the nascent strand of DNA both *in vitro* and *in vivo* (*19*, *42*, *43*). Figure 7 shows a linear sequence of RPA domains binding for simplicity. It seems likely that there are multiple kinetic pathways of RPA binding and that the interactions of the lower-affinity DBDs in RPA will depend on the context of the DNA being bound.

NOTE ADDED IN PROOF

A. I. Arunkumar and co-workers (in press in *Journal of Biological Chemistry*) have also examined DNA binding of the core domains of RPA and found that DBD A binds DNA with higher affinity than DBD B.

ACKNOWLEDGMENT

We thank the members of the Wold laboratory for scientific discussions and critical reading of the manuscript. We thank The University of Iowa DNA Core Facility for oligonucleotide synthesis and DNA sequencing andThe University of Iowa Molecular Analysis Facility for mass analysis. We thank Dr. Jason Telford, University of Iowa, for the use of his CD spectrophotometer.

REFERENCES

1. Iftode, C., Daniely, Y., and Borowiec, J. A. (1999) *CRC Crit. Rev. Biochem. 34*, 141−180.
2. Wold, M. S. (1997) *Annu. Rev. Biochem. 66*, 61−92.
3. Wold, M. S., and Kelly, T. (1988) *Proc. Natl. Acad. Sci. U.S.A. 85*, 2523−2527.
4. Wobbe, C. R., Weissbach, L., Borowiec, J. A., Dean, F. B., Murakami, Y., Bullock, P., and Hurwitz, J. (1987) *Proc. Natl. Acad. Sci. U.S.A. 84*, 1834−1838.
5. Fairman, M. P., and Stillman, B. (1988) *EMBO J. 7*, 1211−1218.
6. Ishibashi, T., Kimura, S., Furukawa, T., Hatanaka, M., Hashimoto, J., and Sakaguchia, K. (2001) *Gene 272* (1−2), 335−343.
7. Heyer, W.-D., Rao, M. R. S., Erdile, L. F., Kelly, T. J., and Kolodner, R. D. (1990) *EMBO J. 9*, 2321−2329.
8. Brill, S. J., and Stillman, B. (1991) *Genes Dev. 5*, 1589−1600.
9. Murzin, A. G. (1993) *EMBO J. 12*, 861−867.
10. Philipova, D., Mullen, J. R., Maniar, H. S., Gu, C., and Brill, S. J. (1996) *Genes Dev. 10*, 2222−2233.
11. Bochkarev, A., Pfuetzner, R. A., Edwards, A. M., and Frappier, L. (1997) *Nature 385*, 176−181.
12. Bochkarev, A., Bochkareva, E., Frappier, L., and Edwards, A. M. (1999) *EMBO J. 18*, 4498−4504.
13. Jacobs, D. M., Lipton, A. S., Isern, N. G., Daughdrill, G. W., Lowry, D. F., Gomes, X., and Wold, M. S. (1999) *J. Biomol. NMR 14*, 321−331.
14. Bochkareva, E., Korolev, S., Lees-Miller, S. P., and Bochkarev, A. (2002) *EMBO J. 21*, 1855−1863.
15. Braun, K. A., Lao, Y., He, Z., Ingles, C. J., and Wold, M. S. (1997) *Biochemistry 36*, 8443−8454.

16. Daughdrill, G. W., Ackerman, J., Isern, N. G., Botuyan, M. V., Arrowsmith, C., Wold, M. S., and Lowry, D. F. (2001) *Nucleic Acids Res. 29*, 3270−3276.
17. Walther, A. P., Gomes, X. V., Lao, Y., Lee, C. G., and Wold, M. S. (1999) *Biochemistry 38*, 3963−3973.
18. Lao, Y., Gomes, X. V., Ren, Y. J., Taylor, J. S., and Wold, M. S. (2000) *Biochemistry 39*, 850−859.
19. Pestryakov, P. E., Weisshart, K., Schlott, B., Khodyreva, S. N., Kremmer, E., Grosse, F., Lavrik, O. I., and Nasheuer, H. P. (2003) *J. Biol. Chem. 278*, 17515−17524.
20. Lao, Y., Lee, C. G., and Wold, M. S. (1999) *Biochemistry 38*, 3963−3973.
21. Kim, C., Paulus, B. F., and Wold, M. S. (1994) *Biochemistry 33*, 14197−14206.
22. Kim, C., and Wold, M. S. (1995) *Biochemistry 34*, 2058−2064.
23. Bhattacharya, S., Botuyan, M. V., Hsu, F., Shan, X., Arunkumar, A. I., Arrowsmith, C. H., Edwards, A. M., and Chazin, W. J. (2002) *Protein Sci. 11*, 2316−2325.
24. Bastin-Shanower, S. A., and Brill, S. J. (2001) *J. Biol. Chem. 276*, 36446−36453.
25. Ausubel, F. M., Brent, R., Kingston, R. E., Moore, D. D., Seidman, J. G., Smith, J. A., and Struhl, K. (1989) *Current protocols in molecular biology*, Wiley, New York.
26. Henricksen, L. A., Umbricht, C. B., and Wold, M. S. (1994) *J. Biol. Chem. 269*, 11121−11132.
27. Walther, A. P. (2000) Replication Protein A: Role in the Elongation Phase of DNA Replication and Function in Cellular Response to DNA Damage, Ph.D. Dissertation, The University of Iowa, Iowa City, IA.
28. Kim, C., Snyder, R. O., and Wold, M. S. (1992) *Mol. Cell. Biol. 12*, 3050−3059.
29. Gomes, X. V., and Wold, M. S. (1995) *J. Biol. Chem. 270*, 4534−4543.
30. Brill, S. J., and Bastin-Shanower, S. (1998) *Mol. Cell. Biol. 18*, 7225−7234.
31. Gomes, X. V., Henricksen, L. A., and Wold, M. S. (1996) *Biochemistry 35*, 5586−5595.
32. Lohman, T. M., and Ferrari, M. E. (1994) *Annu. Rev. Biochem. 63*, 527−570.
33. Raghunathan, S., Kozlov, A. G., Lohman, T. M., and Waksman, G. (2000) *Nat. Struct. Biol. 7*, 648−652.
34. Raghunathan, S., Ricard, C. S., Lohman, T. M., and Waksman, G. (1997) *Proc. Natl. Acad. Sci. U.S.A. 94*, 6652−6657.
35. Webster, G., Genschel, J., Curth, U., Urbanke, C., Kang, C. H., and Hilgenfeld, R. (1997) *FEBS Lett. 411*, 313−316.
36. Yang, H., Jeffrey, P. D., Miller, J., Kinnucan, E., Sun, Y., Thoma, N. H., Zheng, N., Chen, P. L., Lee, W. H., and Pavletich, N. P. (2002) *Science 5588*, 1837−1848.
37. Van der Knaap, E., Jagoueix, S., and Kende, H. (1997) *Proc. Natl. Acad. Sci. U.S.A. 94*, 9979−9983.
38. De Laat, W. L., Appeldoorn, E., Sugasawa, K., Weterings, E., Jaspers, N. G. J., and Hoeijmakers, J. H. J. (1998) *Genes Dev. 12*, 2598−2609.
39. Iftode, C., and Borowiec, J. A. (2000) *Biochemistry 39*, 11970−11981.
40. Patrick, S. M., and Turchi, J. J. (2001) *J. Biol. Chem. 276* (25), 22630−22637.
41. Lao, Y., Gomes, X. V., Ren, Y. J., Taylor, J. S., and Wold, M. S. (2000) *Biochemistry 39*, 850−859.
42. Kolpashchikov, D. M., Weisshart, K., Nasheuer, H. P., Khodyreva, S. N., Fanning, E., Favre, A., and Lavrik, O. I. (1999) *FEBS Lett. 450*, 131−134.
43. Mass, G., Nethanel, T., Lavrik, O. I., Wold, M. S., and Kaufmann, G. (2001) *Nucleic Acids Res. 29* (18), 3892−3899.

BI034930H